Split supersymmetry at colliders

W. Kilian[1,a], T. Plehn[2,b], P. Richardson[3,c], E. Schmidt[4,d]

[1] Deutsches Elektronen-Synchrotron DESY, 22603 Hamburg, Germany
[2] CERN, 1211 Geneva 23, Switzerland
[3] Institute for Particle Physics Phenomenology, University of Durham, DH1 3LE, UK
[4] Fachbereich Physik, University of Rostock, 18051 Rostock, Germany

Abstract. We consider the collider phenomenology of split-supersymmetry models. Despite the challenging nature of the signals in these models the long-lived gluino can be discovered with masses above 2 TeV at the LHC. At a future linear collider we will be able to observe the renormalization group effects from split supersymmetry, using measurements of the neutralino and chargino masses and cross sections.

1 Introduction

The standard signatures of supersymmetry at a hadron collider consist of multi-jet and multi-lepton final states with missing transverse energy [1]. The underlying physics typically involves pair production of new heavy colored particles (squarks and gluinos), which cascade decay into the lightest supersymmetric particle (LSP). This particle, also a dark-matter candidate, leaves the detector undetected. In standard supergravity-mediated models [2], it is the lightest neutralino, while in gauge-mediated supersymmetry-breaking models [3] the gravitino plays this role.

This type of phenomenology naturally appears in hidden-sector models of supersymmetry breaking. If there is a large mass gap between the electroweak scale and the lowest new-physics scale, where new particles interact directly with the visible sector, the MSSM is the correct effective theory over many orders of magnitude (modulo fine-tuning arguments). In the MSSM, the renormalization group flow drives the masses of the colored particles to comparatively large values, while the weakly-interacting states stay relatively light, but all particles are expected to have masses below a few TeV [4].

However, the actual supersymmetric spectrum need not follow this generic expectation. For instance, there are scenarios where the gluino is the LSP [5,6]. If the gluino is long-lived, it will pick up quarks and gluons from the vacuum and hadronize into a (meta)stable R-hadron [5]. In that case, the SUSY signal no longer consists of missing energy in the hard process. Instead, there will be atypical hits in the hadronic calorimeter (and in other parts of the

detector). These correspond to a R-hadron, which either is stopped in or passes through the detector, possibly leaving a fake missing-energy signal.

Recently, this feature has appeared in the context of (SpS) models [7,8]. It is a well-known fact that all known models of electroweak symmetry breaking, including supersymmetric ones, require an incredible amount of fine-tuning of the vacuum energy, such that the resulting cosmological constant is as small as observed. Weakly interacting models, which contain a Higgs boson, require somewhat less, but still incredible additional fine-tuning of the electroweak scale. The latter hierarchy problem is ameliorated in models with exact cancellations in the Higgs sector quantum corrections due to TeV-scale new particles. Softly broken supersymmetry achieves this to all orders in the coupling constants. However, if we accept the fine-tuning of the vacuum energy without explanation, fine-tuning of the electroweak scale does not really worsen the problem. The solution to both hierarchy problems might not involve natural cancellations but follow from a completely different reasoning, such as the idea that galaxy and star formation, chemistry and biology, are simply impossible without these scales having the values found in our Universe [9]. In the vast landscape of possible string theory vacua, we may find ourselves in the observed ground state for exactly these reasons [10].

Supersymmetry has other merits: R-parity provides a natural dark-matter candidate with about the right properties. Grand unification is achieved by the quantum corrections due to the gauginos and Higgsinos. However, supersymmetry has problems as well: naturalness is again in conflict with experiment, since the non-observation of light Higgs bosons and gauginos at LEP requires large, somewhat fine-tuned, soft-breaking parameters. Large flavor-changing neutral current (FCNC) effects due to sfermion exchange are generically expected but not observed, a prob-

[a] e-mail: wolfgang.kilian@desy.de
[b] e-mail: tilman.plehn@cern.ch
[c] e-mail: peter.richardson@durham.ac.uk
[d] e-mail: schmidt@rubin.physik2.uni-rostock.de
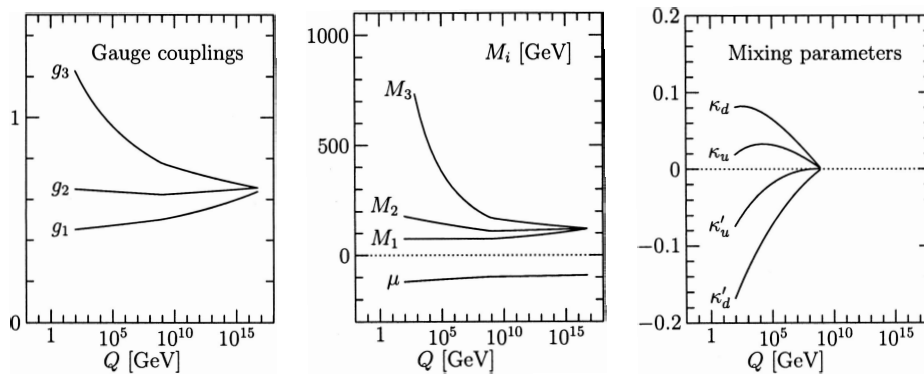
Fig. 1. Renormalization group flow of the gauge couplings (left), the gaugino–Higgsino mass parameters (centre), and the anomalous gaugino–Higgsino mixing parameters defined in (4) (right). All curves are based on our reference point (2)

lem that only has a natural solution in gauge-mediated models. It is also possible that dimension-five operators at the GUT scale could mediate proton decay with an unacceptable rate.

Giving up naturalness of the electroweak scale, the SpS scenario solves the problems without sacrificing the merits. If all sfermions are heavy, it is well known that the pattern of grand unification is unchanged, since they form complete SU(5) representations [11]. The Higgs bosons are also expected to be heavy, but by fine-tuning the B term in the Higgs potential the one Higgs doublet of the standard model can be made light. This modification of the MSSM spectrum does not necessarily affect the mass parameters of gauginos and Higgsinos, which can be protected by the combination of R symmetry and Peccei–Quinn symmetries. Hence, a TeV-scale LSP is possible (albeit not guaranteed). In the absence of light sfermions, the FCNC and proton-decay problems completely disappear.

The low-energy effective theory is particularly simple. In addition to the standard model spectrum including the Higgs boson, the only extra particles are the four neutralinos, two charginos and a gluino. Since all squarks are very heavy the gluino is long-lived. Renormalization group running without sfermions and heavy Higgs bosons lifts the light Higgs mass considerably above the LEP limit, solving another problem of the MSSM. Still, the Higgs boson is expected to be lighter than about 200 GeV [7, 8]. Apart from this Higgs mass bound, the only trace of supersymmetry would be the mutual interactions of Higgs bosons, gauginos and Higgsinos, i.e. the chargino and neutralino Yukawa couplings. These couplings are determined by the gauge couplings at the matching scale $\widetilde{m}$, where the scalars are integrated out. Renormalization group running yields corrections of the order of 10–20% for these couplings [8,12].

At the LHC, the experimental challenge would be the observation and classification of the R-hadrons. In addition, we would like to search for direct production of the charginos and neutralinos, to identify their gaugino and Higgsino components, and to measure their Higgs Yukawa couplings. The absence of scalar states can be checked by constraining contact terms. Obviously, these precision measurements are a perfect task for a high-luminosity linear collider.

2 Renormalization group evolution

In supergravity-inspired SpS models, grand unification relates the bino, wino and gluino mass parameters $M_{1,2,3}$ at a high scale. The constraint that the LSP should not overclose the Universe requires μ to be not much larger than M_1 or M_2 [8,13]. At low energies, the SpS renormalization group enhances the splitting between M_1 and M_2 on one side and M_3 on the other side with respect to the MSSM. The gluino will be heavy in comparison to the neutralinos and charginos. All neutralinos and charginos are strongly mixed, because the μ parameter should be chosen small at the high scale and then stays small after renormalization group running.

Assuming gaugino mass unification and a small Higgsino mass parameter, we start from the following model parameters at the grand unification scale $M_{\mathrm{GUT}} = 6 \times 10^{16}$ GeV:

$$M_1(M_{\mathrm{GUT}}) = M_2(M_{\mathrm{GUT}}) = M_3(M_{\mathrm{GUT}}) = 120\,\mathrm{GeV}\,,$$
$$\tan\beta = 4\,. \tag{1}$$

For the SUSY-breaking scale we choose $\widetilde{m} = 10^9$ GeV[1]. In the effective theory approach this is the intermediate matching scale where the scalars are integrated out. Figure 1 displays the solutions of the renormalization group equations [14] following the appendix of [8] with the input parameters set in (1). At the low scale $Q = m_Z$, we extract the mass parameters:

$$M_1(Q = m_Z) = 74.8\,\overline{\mathrm{DR}}(Q = 1\,\mathrm{GeV})\,,$$
$$M_2(Q = m_Z) = 178.1\,\mathrm{GeV}\,. \tag{2}$$

The resulting physical gaugino and Higgsino masses are

$$m_{\tilde{\chi}_1^0} = 71.1\,\tilde{\chi}_1^+ = 114.7\,\tilde{\chi}_2^0 = 109.9\,\tilde{\chi}_2^+$$
$$= 215.7\,\tilde{\chi}_3^0 = 141.7\,\tilde{\chi}_4^0 = 213.7\,\tilde{g} = 807\,. \tag{3}$$

These mass values satisfy the LEP constraints. The neutralinos $\tilde{\chi}_{1,2,3,4}^0$ are predominantly bino, Higgsino, Higgsino, and wino, respectively. The Higgsino content of the

---

[1] We stress that the phenomenology for this particular choice of $\widetilde{m}$ is identical to the case $\widetilde{m} = M_{\mathrm{GUT}}$, as will become obvious during the analysis.

lightest neutralino is $h_f = 0.2$, so the dark-matter condition [13] is satisfied. To our given order the Higgs mass is $m_H = 150\,\text{GeV}$, but as usually it will receive sizable radiative corrections [15].

Because we integrate out the heavy scalars, the neutralino and chargino Yukawa couplings deviate from their usual MSSM prediction, parameterized by four anomalous Yukawa couplings κ [12]. We can extract their weak-scale values from Fig. 1:

$$\frac{\tilde{g}_u}{g \sin \beta} \equiv 1 + \kappa_u = 1 + 0.018\,,$$

$$\frac{\tilde{g}_d}{g \cos \beta} \equiv 1 + \kappa_d = 1 + 0.081\,,$$

$$\frac{\tilde{g}'_u}{g' \sin \beta} \equiv 1 + \kappa'_u = 1 - 0.075\,,$$

$$\frac{\tilde{g}'_d}{g' \cos \beta} \equiv 1 + \kappa'_d = 1 - 0.17\,. \tag{4}$$

Note that these are the leading logarithmic renormalization group effects, which should be supplemented by the complete one-loop corrections to the neutralino and chargino mixing matrices [16].

3 Signals at the LHC

The production cross section of gluinos and of charginos and neutralinos at the LHC are known to NLO [17]. In SpS models these cross sections depend only on the gluino mass and the chargino and neutralino masses and mixings, respectively, the latter being determined by the gaugino mass parameters M_1 and M_2 and the Higgsino mass μ. In Table 1 we list the LHC production cross sections for our example parameter point in (3). For neutralino pairs we can understand the simple pattern, since in the heavy squark limit, neutralino production only proceeds through a Drell–Yan s-channel Z boson. The neutralinos with a large Higgsino fraction are $\tilde{\chi}^0_{2,3}$, which makes the $\tilde{\chi}^0_2 \tilde{\chi}^0_3$ production dominant. The pair production of either of these two states is
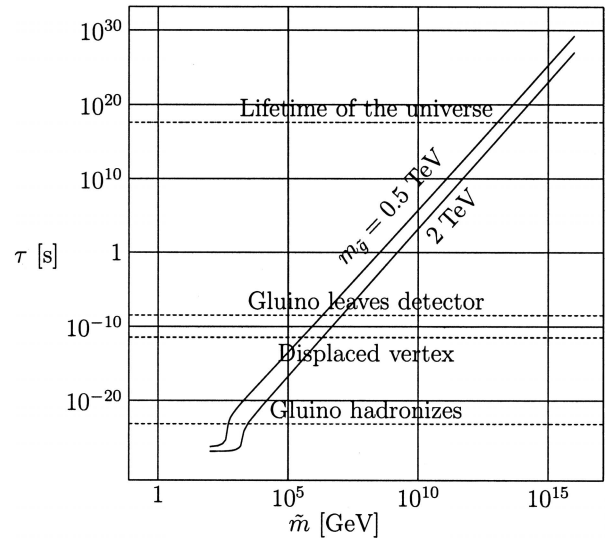
suppressed because the couplings of the Z boson to the two Higgsino states cancel each other in the superposition. Diagonal chargino pairs are produced at a comparably large rate because of the s-channel photon exchange.

The charginos are strongly mixed, but the ligher $\tilde{\chi}^\pm_1$ has a larger Higgsino and the heavier $\tilde{\chi}^\pm_2$ has a larger wino fraction. In mixed chargino and neutralino production, the s-channel W boson couples to either a $\tilde{H}^0 \tilde{H}^\pm$ or to a $\tilde{W}^0 \tilde{W}^\pm$ combination. Because of the composition of the neutralinos, the production cross sections for $\tilde{\chi}^\pm_1 \tilde{\chi}^0_2$, $\tilde{\chi}^\pm_1 \tilde{\chi}^0_3$, and $\tilde{\chi}^\pm_2 \tilde{\chi}^0_4$ are dominant (the combination of the lightest chargino and neutralino benefits from their small masses and the sizable mixing). The final states with a positive charge have a typically twice as large a cross section as the final states with negative charge, due to the valence quark decomposition of the initial-state proton.

Strategies to discover MSSM particles and measure their masses at the LHC usually rely on the production of squarks and gluinos and subsequent cascade decays to the weakly-interacting superpartners. In SpS scenarios this is not possible. Instead, we have to look for direct Drell–Yan-like production channels, which are plagued by overwhelming W and Z production backgrounds. In particular the trilepton signature $pp \to \tilde{\chi}^0_2 \tilde{\chi}^+_1$ becomes considerably harder to observe if the decay $\tilde{\chi}^0_2 \to \ell^+ \ell^- \tilde{\chi}^0_1$ does not involve an intermediate slepton. Our SpS parameter point with the masses given in (3) does not allow for the decay $\tilde{\chi}^0_2 \to H \tilde{\chi}^0_1$, but for heavier particles this decay might be promising to look for gauginos and Higgsinos at the LHC. Note that the associated production of charginos and neutralinos with a gluino is mediated by a t-channel squark exchange and therefore is suppressed.

3.1 Gluino decays

Unless we have a priori knowledge about the sfermion scale $\tilde{m}$, the gluino lifetime is undetermined. Figure 2 compares

Table 1. NLO production cross sections at the LHC [17]. The masses and mixing matrices are fixed by the reference point in (2)

	σ [fb]		σ [fb]		σ [fb]		σ [fb]
$\tilde{g}\tilde{g}$	1710						
$\tilde{\chi}^-_1 \tilde{\chi}^+_1$	2910	$\tilde{\chi}^-_1 \tilde{\chi}^+_2$	73.7	$\tilde{\chi}^+_1 \tilde{\chi}^-_2$	73.7	$\tilde{\chi}^+_2 \tilde{\chi}^-_2$	604
$\tilde{\chi}^0_1 \tilde{\chi}^0_1$	49.4	$\tilde{\chi}^0_1 \tilde{\chi}^0_2$	49.7	$\tilde{\chi}^0_1 \tilde{\chi}^0_3$	409	$\tilde{\chi}^0_1 \tilde{\chi}^0_4$	0.06
		$\tilde{\chi}^0_2 \tilde{\chi}^0_2$	5.0	$\tilde{\chi}^0_2 \tilde{\chi}^0_3$	876	$\tilde{\chi}^0_2 \tilde{\chi}^0_4$	3.7
				$\tilde{\chi}^0_3 \tilde{\chi}^0_3$	1.4	$\tilde{\chi}^0_3 \tilde{\chi}^0_4$	69.6
						$\tilde{\chi}^0_4 \tilde{\chi}^0_4$	1.0
$\tilde{\chi}^-_1 \tilde{\chi}^0_1$	584	$\tilde{\chi}^-_1 \tilde{\chi}^0_2$	1780	$\tilde{\chi}^-_1 \tilde{\chi}^0_3$	789	$\tilde{\chi}^-_1 \tilde{\chi}^0_4$	78.8
$\tilde{\chi}^+_1 \tilde{\chi}^0_1$	914	$\tilde{\chi}^+_1 \tilde{\chi}^0_2$	2870	$\tilde{\chi}^+_1 \tilde{\chi}^0_3$	1310	$\tilde{\chi}^+_1 \tilde{\chi}^0_4$	138
$\tilde{\chi}^-_2 \tilde{\chi}^0_1$	2.7	$\tilde{\chi}^-_2 \tilde{\chi}^0_2$	55.9	$\tilde{\chi}^-_2 \tilde{\chi}^0_3$	66.6	$\tilde{\chi}^-_2 \tilde{\chi}^0_4$	430
$\tilde{\chi}^+_2 \tilde{\chi}^0_1$	4.5	$\tilde{\chi}^+_2 \tilde{\chi}^0_2$	97.7	$\tilde{\chi}^+_2 \tilde{\chi}^0_3$	119	$\tilde{\chi}^+_2 \tilde{\chi}^0_4$	798

Fig. 2. Gluino lifetime [18] as a function of the common scalar mass $\tilde{m}$

this scale with other relevant scales of particle physics. Once $\widetilde{m} \gtrsim 10^3 \,\mathrm{GeV}$, the gluino hadronizes before decaying. For $\widetilde{m} > 10^6 \,\mathrm{GeV}$, weak decays of heavy-flavored R-hadrons start to play a role, and the gluino travels a macroscopic distance. If $\widetilde{m} > 10^7 \,\mathrm{GeV}$, strange R-hadrons can also decay weakly, and gluinos typically leave the detector undecayed or are stopped in the material. For even higher scales, $\widetilde{m} > 10^9 \,\mathrm{GeV}$, R-hadrons could become cosmologically relevant, since they affect nucleosynthesis if their abundance in the early Universe is sufficiently high [7,8]. Finally, $\widetilde{m} > 10^{13} \,\mathrm{GeV}$ is equivalent to a stable gluino since its lifetime is longer than the age of the Universe. With the given value of the intermediate scale $\widetilde{m} = 10^9 \,\mathrm{GeV}$ and the weak-scale parameters of (2), the gluino width is of the order of

$$\Gamma_{\tilde{g}} \approx 1.0 \times 10^{-25} \,\mathrm{GeV}\,, \qquad \text{i.e.} \qquad \tau_{\tilde{g}} \approx 6.5 \,\mathrm{s}\,. \qquad (5)$$

The precise value can be computed only if the detailed squark spectrum is known; the above numbers correspond to universal scalar masses and no mixing.

If gluino decays can be observed, their analysis yields information about physics at the scale $\widetilde{m}$ and thus allows us to draw conclusions about the mechanism of supersymmetry breaking. In a standard MSSM scenario with heavy scalars, the gluino will experience a three-body decay $\tilde{g} \to q\bar{q}\tilde{\chi}^0$ or $\tilde{g} \to q\bar{q}'\tilde{\chi}^\pm$. The $\tilde{\chi}$'s are predominantly gaugino for light quarks in the final state. In the charged decay, the flavor mixing is governed by the standard CKM matrix. A loop-induced decay $\tilde{g} \to g\tilde{\chi}^0$ is also possible and has a rate comparable to the tree-level three-body decays. This decay mainly proceeds via a top/stop loop, and the neutralino is predominantly Higgsino.

In the usual MSSM scenarios squarks are degenerate, so these decays are flavor-diagonal modulo CKM effects and left–right squark mixing in the third generation. The situation is different in SpS: due to the absence of FCNC constraints, arbitrary sfermion mass patterns are allowed once the scalar mass $\widetilde{m}$ exceeds a value of order $10^5 \,\mathrm{GeV}$. On the other hand, the left–right sfermion mixing angles vanish in SpS since the off-diagonal elements of the mixing matrices are suppressed by $v/\widetilde{m}$. Therefore, the flavor decomposition of gluino decays mirrors the sfermion mass hierarchy at the matching scale $\widetilde{m}$. The ratio of branching ratios $\tilde{g} \to q\bar{q}\tilde{\chi}^0$ and $\tilde{g} \to Q\bar{Q}\tilde{\chi}^0$ is given by $(m_{\tilde{Q}}/m_{\tilde{q}})^4$, so even a weak hierarchy will be greatly enhanced in the branching ratios. If the decays of long-lived gluinos can be observed, it is important to identify flavor, even though the conditions of flavor-tagging are non-standard if the decay does not occur near the interaction point.

3.2 R-hadrons

R-hadrons have been discussed early in supersymmetry phenomenology [5]. The spectrum of light-flavored R-hadrons can be computed using a bag model [19] or lattice calculations [20]. The gluino is a color octet; therefore a color-singlet hadron can be made by adding a quark–antiquark pair coupled as an octet (in SU(3), $3 \otimes \bar{3} = 8 \oplus 1$),

or by three quarks coupled as an octet, which is possible in two ways ($3 \otimes 3 \otimes 3 = 10 \oplus 8 \oplus 8' \oplus 1$). Furthermore, the gluino color can be neutralized by adding a single constituent gluon (or another gluino, for that matter). These neutral states are collectively denoted by R_g. In any case, for a heavy gluino the mass differences of the various R states are small with respect to the overall mass. This situation is described by heavy-quark effective theory, where the gluino acts as a static color source, unaffected by the dynamics of the quark–gluon cloud around it [21].

The $\tilde{g}\bar{q}q$ hadrons are similar to ordinary mesons, and they may be labelled in an analogous way: $R_\pi, R_\rho, R_K, \dots$ The total spin is fermionic (1/2 or 3/2), but this does not affect the dynamics because the gluino spin decouples from the surrounding cloud and a meson description is therefore appropriate. The higher excitations rapidly decay into the lowest excitations. Considering the ground states, we note that the R_π hadrons are not Goldstone bosons, so they are not particularly light. The numerical estimates in [20] indicate that the R_ρ states are slightly lighter, and the lowest R_g is close to it. However, all mass differences are expected to be less than 100 MeV, so that all these ground states are stable with respect to the strong interaction. As long as the gluino decays at all, there is no reason for the lowest state to be neutral, so after weak decays the final state of the R-hadron decay chain could be either a neutral R or, say, the $R_\rho^\pm$. In analogy to the mixing of the ρ^0 and the photon, we expect mixing of R_ρ^0 and R_g, so there may be significant isospin-breaking effects.

The R-baryon spectrum differs considerably from ordinary baryons by the different color- and flavor-coupling schemes allowed. Their spectrum can be estimated using bag models [22]. However, in the process of fragmentation, baryon formation is less likely than meson formation, a feature that should persist in the present situation.

If the gluino production rate is sufficiently large, heavy-flavored R-hadrons can be produced. These are interesting objects, because their weak decays may provide distinctive signatures of SpS. Let us consider the $R_B^- = \tilde{g}b\bar{u}$. In the field of the static source $\tilde{g}$, the b quark will tightly bind to it, since $m_b \gg \Lambda_{\mathrm{QCD}}$. This system is approximately described by the same perturbative potential as describes the lowest-lying Υ states. The difference is that the physical b mass should be used instead of the reduced mass $m_b/2$, and therefore α_s should be evaluated at a slightly higher scale. Moreover, the prefactor 4/3, which is appropriate for $3 \otimes \bar{3} \to 1$ coupling we must replace by 3/2, which corresponds to $8 \otimes 3 \to 3$. (Note that the triplet channel is the most attractive one in the coupling of an octet and a singlet.) Assuming that the systems are Coulombic, we can estimate the R_b binding energy:

$$E(R_b) \approx \frac{9}{4} \frac{\alpha(m_b)}{\alpha(m_b/2)} E(\Upsilon) \qquad (6)$$

If we take $m_{\Upsilon(1S)} - 2m_B = -1 \,\mathrm{GeV}$ as the Υ binding energy, we obtain $E(R_b) \approx -2 \,\mathrm{GeV}$. Clearly, this estimate can be refined by looking at the potential in more detail.

The gluino–b system forms a color-triplet nucleus, which is surrounded by the light-quark cloud. Heavy-quark sym-

metry tells us that the dynamics of this cloud is similar to the dynamics of an ordinary B-meson. More precisely, the orbital part of the Hamiltonian is the HQET Hamiltonian in the extreme heavy-mass limit. The spin part is identical to the B-meson Hamiltonian, since only the b-quark spin couples to the light cloud, suppressed by $\Lambda_{\rm QCD}/m_b$, while the gluino spin is irrelevant. Thus, B-meson data can be exploited to determine many of the properties of these states.

3.3 Long-lived gluinos at the LHC

The phenomenology of SpS models at the LHC is very dependent on the lifetime of the gluino. If this is smaller than the hadronization time scale, the signals will be the usual signals for supersymmetry [1]. If the gluino hadronizes, but the lifetime of the R-hadrons produced is short enough that they decay inside the detector, we might see additional vertices from the R-hadron decay. Because the phenomenology of these scenarios has been extensively considered in the literature, we will only consider the long-lived gluino here. For a stable R-hadron we investigate two types of signals. (1) The production of a stable, charged, R-hadron will give a signal much like the production of a stable charged weakly-interacting particle [23, 24]. This signal consists of an object that looks like a muon but arrives at the muon chambers significantly later than a muon owing to its large mass. However, the situation will be more complicated than those considered in [23, 24], as the R-hadron will interact more in the detector, losing more energy.
(2) While for stable neutral R-hadrons there will be some energy loss in the detector, there will be a missing transverse energy signal due to the escape of the R-hadrons. As leptons are unlikely to be produced in this process the signal will be the classic SUSY jets with missing transverse energy signature.

There is also the possibility of signals involving the production and semileptonic decay of R-hadrons containing a heavy, i.e. bottom or charm, quark. For a gluino, which is stable on collider time scales, the phenomenology of the model depends on the cross section, which is controlled by the gluino mass, the ratio of stable charged to neutral R-hadrons produced and, for the decay of R-hadrons containing a heavy quark, the number of these hadrons produced.

To study the production of R-hadrons at the LHC we have to model the hadronization of the gluino. Our simulations use the HERWIG Monte Carlo event generator [25], which in turn uses the cluster hadronization model [26]. In HERWIG, the gluons left at the end of the perturbative evolution in the QCD parton shower are non-perturbatively split into quark–antiquark pairs. In the large-N_C limit, the quarks and antiquarks can be uniquely formed into color-singlet clusters that carry mesonic quantum numbers. Preconfinement ensures that these clusters have a mass spectrum that peaks at low values and falls off rapidly at higher masses.

These clusters are assumed to be a superposition of the known hadron resonances and decay into two hadrons.

To illustrate the decay we consider a cluster containing a quark q_i and an antiquark $\bar{q}_j$ (i, j are flavor indices). First, a quark–antiquark pair of flavor k is produced from the vacuum with probability $P_k{}^2$. This specifies the flavors of the two produced mesons, $(q_i\bar{q}_k)$ and $(q_k\bar{q}_j)$. The type of meson is randomly chosen from the available mesons with the correct flavors. A weight

$$W = (2S_{q_i\bar{q}_k}+1)\,(2S_{q_k\bar{q}_j}+1)\,\Phi\left[C \to (q_i\bar{q}_k),(q_k\bar{q}_j)\right]\,, \quad (7)$$

where $S_{q_i\bar{q}_k}$ and $S_{q_k\bar{q}_j}$ are the spins of the mesons selected and $\Phi\left[C \to (q_i\bar{q}_k),(q_k\bar{q}_j)\right]$ is the two-body phase-space weight for the decay of the cluster, is then calculated. A decay is accepted if $W \geq \mathcal{R}W_{\max}$ where $\mathcal{R}$ is a random number between 0 and 1 and $W_{\max}$ is the maximum possible weight. If the decay is rejected the procedure is repeated and a new quark–antiquark pair and new types of mesons are selected.

If we include a gluino, which is stable on the hadronization time scale, we will have a cluster containing a gluino in addition to the quark q_i and the antiquark $\bar{q}_j$. The simplest approach would be to select a quark–antiquark pair $(q_k\bar{q}_k)$ as before, and randomly select either $(q_i\tilde{g}\bar{q}_k)$ and $(q_k\bar{q}_j)$ or $(q_i\bar{q}_k)$ and $(q_k\tilde{g}\bar{q}_j)$ as the flavors for the mesons. However this would forbid direct production of the R_g hadrons and in particular the lightest R-hadron state R_g^0. There is no obvious mechanism for the production of the R_g states in the cluster model; we therefore chose to model R_g production by including the decay of a cluster containing a gluino to R_g and the lightest meson, with quark flavors $(q_i\bar{q}_j)$, in addition to the normal cluster decays. This decay occurs with a probability P_{R_g}. The parameter P_{R_g} will generally act as a parameterization of how many of the R mesons in the detector are neutral and how many are charged. This fraction determines the relative success of the two search strategies listed above.

In order to simplify the simulation we only include the lightest R-hadron with a given quark composition and do not include the R baryons. The lightest R-hadron is taken to be the lightest R_g state (R_g^0) with mass $M_{\tilde{g}}+1.43\,{\rm GeV}$ [27]. The lowest-lying R-meson is the R_ρ with a mass $M_{R_g^0} + 47\,{\rm MeV}$ [20]. The masses of the remaining R-hadrons are then given by

$$M_{R_{q_i\bar{q}_j}} = M_{R_\rho} + m_{q_i} + m_{q_j} - 2m_{u,d}\,, \quad (8)$$

where m_{q_i} is the constituent mass for the quark of flavor i and $m_{u,d}$ is the common constituent mass for the up- and down-type quarks.

The lightest mesonic R_ρ states are taken to be stable, as is the lightest gluonic state R_g^0. The heavier mesonic R-hadrons decay weakly to the appropriate lighter R-hadron and an off-shell W boson, which decays either leptonically or hadronically. The R_ϕ state is too light to have a strong decay and it therefore decays to a pion and the R_ρ, in

---

2 The probabilities P_k are parameters of the model. They are normally set so that the probabilities are equal for the light (up, down and strange) quarks and equal to zero for the heavy (charm and bottom) quarks.

Table 2. Production rates of the R-hadrons. The probability of producing an R_g^0 is set to zero when producing these numbers. The rates of the $R_{q\bar{q}}$ hadrons linearly decrease, and R_g^0 increase, as this probability is increased

R-hadron	$M_{\tilde{g}} = 50\,\mathrm{GeV}$		$M_{\tilde{g}} = 2000\,\mathrm{GeV}$	
	Number per fb^{-1}	Percentage of R-hadrons	Number per fb^{-1}	Percentage of R- hadrons
R_{ρ^0}	$(4.152 \pm 0.006) \times 10^8$	28.10 ± 0.04	0.5576 ± 0.0007	28.22 ± 0.04
R_{ρ^-}	$(2.067 \pm 0.004) \times 10^8$	14.00 ± 0.03	0.2788 ± 0.0005	14.11 ± 0.07
R_{ρ^+}	$(2.076 \pm 0.004) \times 10^8$	14.05 ± 0.03	0.2788 ± 0.0005	14.11 ± 0.07
R_{K^0}	$(1.302 \pm 0.003) \times 10^8$	8.81 ± 0.02	0.1730 ± 0.0004	8.76 ± 0.02
$R_{\bar{K}^0}$	$(1.291 \pm 0.003) \times 10^8$	8.74 ± 0.02	0.1730 ± 0.0004	8.76 ± 0.02
R_{K^+}	$(1.300 \pm 0.003) \times 10^8$	8.80 ± 0.02	0.1728 ± 0.0004	8.75 ± 0.02
R_{K^-}	$(1.299 \pm 0.003) \times 10^8$	8.79 ± 0.02	0.1725 ± 0.0004	8.73 ± 0.02
R_η	$(1.286 \pm 0.003) \times 10^8$	8.71 ± 0.02	0.1687 ± 0.0004	8.54 ± 0.02
R_D	$(2.1 \pm 0.7) \times 10^4$	$(14.5 \pm 2.6) \times 10^{-4}$	$(6.5 \pm 0.8) \times 10^{-5}$	$(3.2 \pm 0.4) \times 10^{-3}$
R_B	$(7 \pm 7) \times 10^3$	$(0.5 \pm 0.5) \times 10^{-4}$	$8.0 \pm 2.8 \times 10^{-6}$	$(0.4 \pm 0.2) \times 10^{-3}$
R_{D_s}	$(20 \pm 4) \times 10^4$	$(14.0 \pm 2.6) \times 10^{-4}$	$4.7 \pm 0.7 \times 10^{-5}$	$(2.4 \pm 0.4) \times 10^{-3}$

analogy with the standard model decay $\phi \to \rho\pi$. The decay of mesons containing a pair of heavy quarks does not need to be modelled, because these are not produced in our approximation.

Assuming both, the R_ρ and the R_g^0 to be stable is based on the observation that their mass difference is smaller than the pion mass. The actual ordering of their masses does not play any role in our analysis. However, the mass difference could of course be much larger. In that case all R-hadrons would decay to one distinctly lightest state. The charge of this final state would in turn decide which of our two search strategies for long-lived gluinos will be successful at the LHC.

The percentages of the different species of R-hadron is shown in Table 2 for two different gluino masses. We see that the $R_{q\bar{q}}$ hadrons containing only light quarks are predominantly produced with a preference for up and down quarks over strange quarks[3]. The production rates for R-hadrons containing a heavy bottom or charm quark is very low. The reason for this is that in our simulation these mesons can only be produced if a gluon that is color-connected to the gluino perturbatively branches into a heavy-quark pair. This might be an underestimate of the production rate for these states; in the same way, HERWIG tends to underestimate the production rates for bottom and charmonium, which are produced by the same mechanism, at LEP energies. However, given the very low rates it is unlikely that there will be enough events to detect a signal based on displaced vertices due to the decay of the companion heavy quark. The information that could be extracted from these decay signatures would of course be highly interesting.

While all these assumptions are necessary to perform the simulations, they do not have a major effect on the

signals we will consider: the phenomenology is mainly determined by the gluino mass and the probability P_{R_g} of producing the R_g^0 rather than an R-meson in the cluster decays.

In addition to the hadronization, we need to consider the interactions of the R-hadrons in the detector. For the interactions of the other particles we use the AcerDet fast simulation [28]. The interaction of the gluino is modelled in the same way as in [6]. The energy and angular dependence of the R-hadron nucleon cross section are modelled using either the cut-off form with a cut-off value of $1\,\mathrm{GeV}$ or the triple-pomeron form considered in Sect. IIIA of [6]. Rather than the approach taken in [6], which uses the average energy loss in these collisions combined with the depth of the detector in terms of radiation lengths, we propagated the R-hadrons through the detector. We generate the distance to the next interaction according to the exponential distribution using the interaction length. The differential cross section is used to calculate the energy loss and change in direction of the R-hadron due to the collision. This gives us fluctuations in the energy loss on an event-by-event basis. For the basic properties of the detector we use the parameters given in Table 3, which are based on the ATLAS detector [29]. The energy loss in the electromagnetic and hadronic calorimeters is added to the cells of the calorimeter of the fast detector simulation. For charged R-hadrons,

---

[3] The difference in production rates between the charged and neutral ρ mesons would be corrected by the inclusion of the R_ω meson. Given our simple modelling this would not affect the results.

Table 3. Size of the detector systems. The size of the components and their depth in terms of interaction lengths are based on the parameters of the ATLAS detector [29]

Detector system	Radius [m]	Length [m]	Number of interaction lengths
Inner detector	1.15	3.5	0.0
Electromagnetic calorimeter	2.25	6.65	1.2
Hadronic calorimeter	4.25	6.65	9.5
Support structure	10	20	1.5
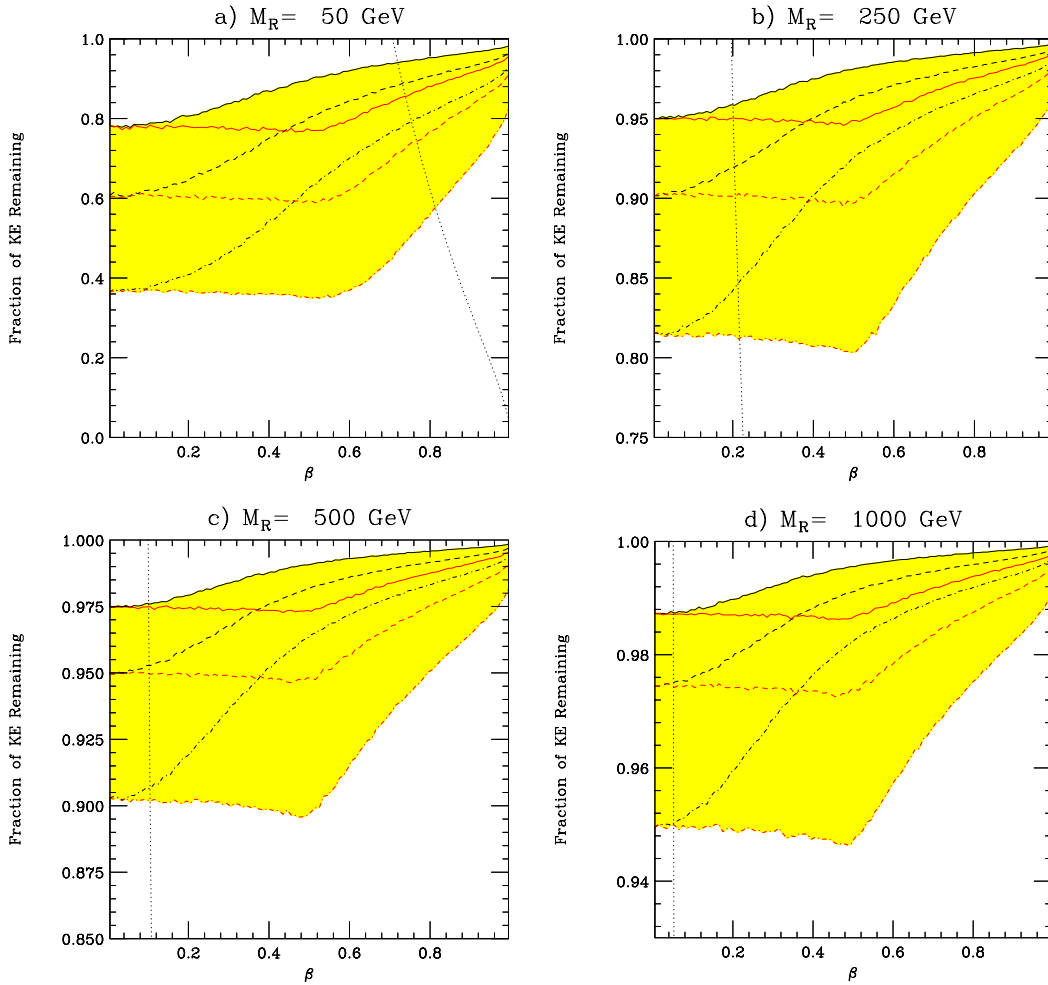
Fig. 3a–d. Fraction of the kinetic energy remaining when the R-hadron enters the muon detector. The black lines are for the triple-pomeron form of the R- hadron nucleon cross section, the red lines are for the simple cut-off form [6]. The interaction length λ_R is varied between twice the central value (solid), the central value (dashed) and half this value (dot-dashed). The dotted line shows where the R-hadron no longer passes the p_T cut for the charged R-hadron analysis

which will be detected in the muon chambers, we assume that the momentum measurement will be dominated by the momentum when the R-hadron reaches the muon chamber. The time of arrival of this meson at the muon chamber is smeared with a Gaussian of width $0.7\,\mathrm{ns}$ [23] and the momentum as described in [23].

Our signatures depend on the energy lost by the R-hadron in the detector. The simple cut-off ansatz for the cross section gives too much energy loss for incident pions, whereas the triple-pomeron form gives a good approximation for pion energies lower than $100\,\mathrm{GeV}$ and too little energy loss at higher energies [6]. We investigate the uncertainty in the modelling of the interaction of the R-hadron with the detector in two ways. The simplest approach is to use the two different models of the cross section. The second is to vary also the interaction length λ_R of the R-hadron in the detector between half and twice the value used in [6]: $\lambda_R \sim 16/9\lambda_\pi$. The effects of these variations are shown in Fig. 3. We find that the size of the variation decreases as the R-hadron mass increases and the effect becomes negligible for the masses we are interested in.

3.3.1 Charged R-hadron searches

We consider two main strategies for the analysis. The first closely follows the analysis in [23] and requires the presence of a charged R-hadron, which is reconstructed as a muon. The transverse momentum of the hadron has to be larger than $50\,\mathrm{GeV}$ (which is sufficient to trigger the event) and the time delay with respect to an ultra-relativistic particle Δt has to satisfy $10\,\mathrm{ns} < \Delta t < 50\,\mathrm{ns}$. An efficiency of 85% is applied for the probability of reconstructing a muon [23].

The mass of the R-hadron can then be reconstructed using

$$m^2 = \frac{p_D \Delta t}{x}\left(2p + \frac{p_D \Delta t}{x}\right), \qquad (9)$$

where p, p_D and x are the momentum, the transverse momentum and radius of the muon detectors or the momentum along the beam direction and half-length of the muon detector, depending on whether the R-hadron hits the barrel or end-cap detectors.

It is important to check what the effect of the modelling of the R-hadron interaction with the calorimeter on the
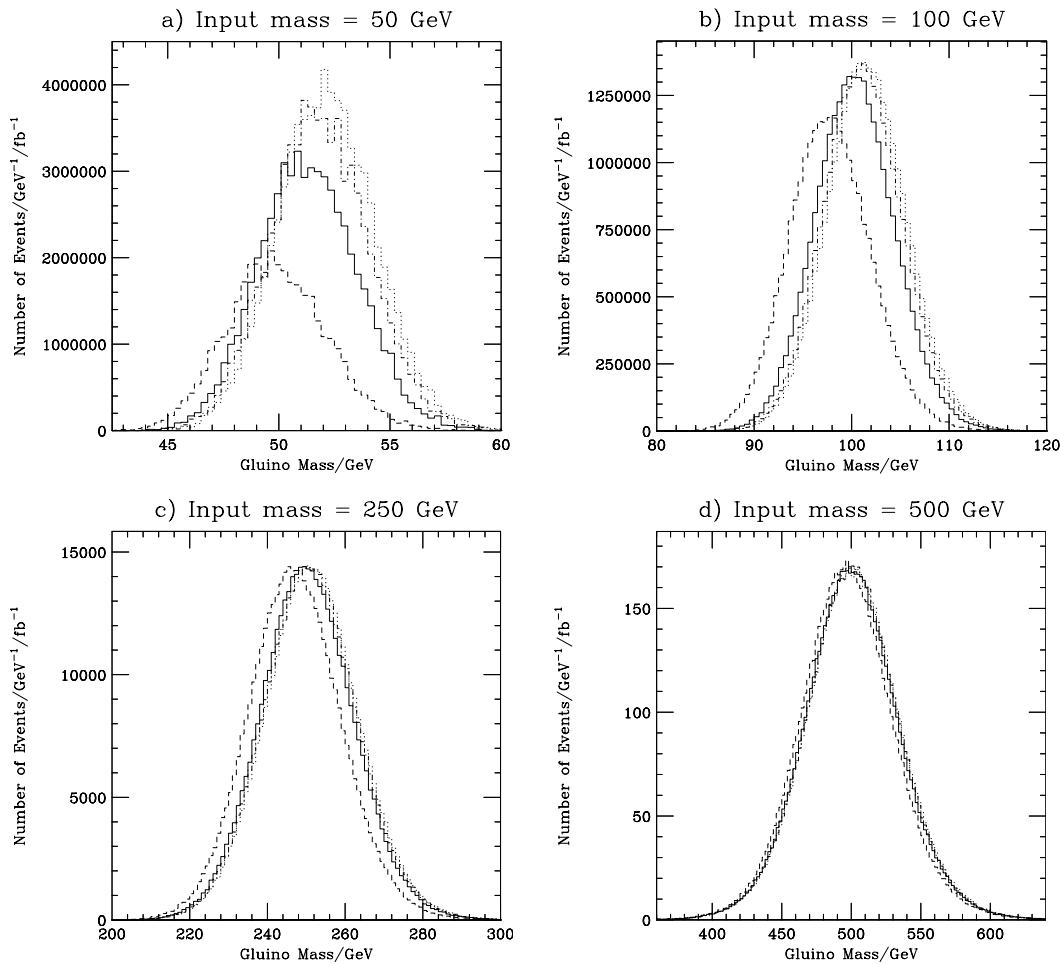
Fig. 4a–d. Effect of the modelling of the interaction with the detector on the reconstructed R-hadron mass for different gluino masses. We show curves for $\lambda_R/2$ with the pomeron cross section form (solid), $\lambda_R/2$ with the cut-off form (dashed), λ_R with the pomeron form (dot-dashed) and $2\lambda_R$ with the pomeron form (dotted). The probability for producing the R_g^0 is set to zero. We simulate one million events, which is less than one year of high-luminosity running for all the masses shown

mass determination is. The reconstructed mass is shown for different gluino masses and choices of the interaction with the calorimeter in Fig. 4. As we expect from Fig. 3 the effects of the different choices of the R-hadron interaction length and cross section are more apparent at low gluino masses. For all masses, halving the interaction length and using the cut-off form of the cross section leads to more energy loss by the R-hadron and hence a lower peak value for the mass and fewer events passing the cuts. For a gluino mass of 50 GeV, the shift in the average mass is 2.3 GeV, for a mass of 500 GeV the shift is 5 GeV, and for a mass of 2 TeV is 6.7 GeV. In a more realistic study this shift could be corrected for by including the energy deposited in the calorimeter when measuring the R-hadron mass.

The cuts we apply should eliminate the standard model background [23]. In order to calculate the discovery reach for charged R-hadrons we require the observation of ten R-hadrons. The results shown in Fig. 3 are using half the default R-hadron interaction length and cut-off form of the R-hadron interaction cross section. This is the model that gives the highest energy loss. However, the results are not particularly sensitive to this choice, and the choice of parameters with the lowest energy loss we consider gives only marginally better results. The reach for this signal is shown in Fig. 5 in the $m_{\tilde{g}}$–P_{R_g} plane. We see that the discovery reach extends to over 1.5 TeV for one year's run-

ning at low luminosity and to over 2 TeV for one year at high luminosity, apart from a region with low probability of producing a mesonic R-hadron.

The resolution of the reconstructed R-hadron mass is shown in Fig. 5 for an integrated luminosity of $100\,\mathrm{fb}^{-1}$. For masses of less than 500 GeV the mass can be measured with a precision of better than 0.05%. For these masses, this precision is better than the shift in the measured mass due to the energy loss of the charged R-hadron in the calorimeter. For higher masses the resolution decreases, but it is still better than 1% for masses up to 1.5 TeV. This is an effect of the mass shift due to the energy loss in the calorimeter.

3.3.2 Neutral R-hadron searches

A second signal that does not depend on the production of charged R-hadrons is the classic jets plus missing transverse energy signature. Neutral R-hadrons will of course always be produced, even if no R_g^0 hadrons are created, because the R_ρ^0 will be produced with the same probability as the charged R-hadrons; see Table 2. For neutral R-hadrons only there will be no production of charged leptons in association with the gluino signal, apart from the decays of heavy hadrons. On the other hand, there will be fake muons from
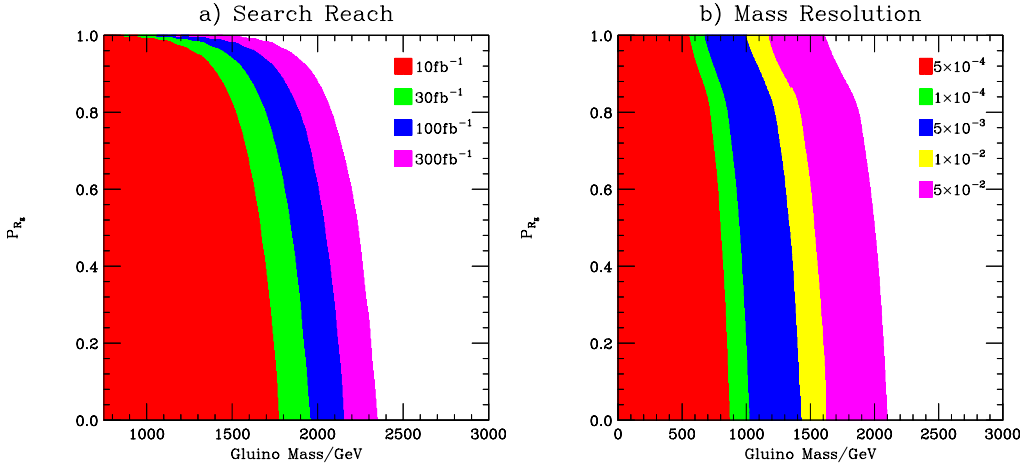
Fig. 5. Discovery reach **a** and mass resolution **b** for charged R-hadrons. We require the observation of ten charged R-hadrons for four different integrated luminosities. We show the mass resolution $\Delta M/M$ for $100\,\mathrm{fb}^{-1}$

the charged R-hadrons. In analysing the missing transverse energy signal we therefore require that there be no leptons in the signal, so as to reduce the background from standard model W and Z production. When applying this cut we assume that charged R-hadrons that pass the same isolation cut as muons will be reconstructed as muons. This is a conservative assumption, because some of them will not be reconstructed, because of the large time delay.

Our approach for neutral R-hadrons is close to that in [30]. The standard model QCD, top quark, W + jets and Z + jets signals are simulated using HERWIG6.5 [25] in logarithmic transverse momentum bins in order to increase the number of events simulated at high-p_{T}, which are most likely to contribute to the background. A number of variables are used to distinguish between the signal and background events:

(1) the missing transverse energy $\not{E}_{\mathrm{T}}$;
(2) the transverse momentum of the hardest jet $P_{\mathrm{T}_{j_1}}$;
(3) the transverse momentum of the second hardest jet $P_{\mathrm{T}_{j_2}}$;
(4) the scalar sum of the transverse momentum of the jets in the event $\sum P_{\mathrm{T}_j}$;
(5) the number of jets N_{jet};
(6) the transverse sphericity of the event S_{T}; see e.g. [1] for the definition of S_{T};
(7) the difference in azimuthal angle between the direction of the hardest jet and $\not{E}_{\mathrm{T}}$.

We test different sets of cuts on these variables to maximize the statistical significance of the signal on a point-by-point basis. The values of the cuts are given in Table 4. The lowest value of the cuts on the missing transverse momentum and on the transverse momentum of the first jet are sufficient for the event to be triggered [30]. We define the significance as $S/\sqrt{S+B}$, to minimize the effect of statistical fluctuations in the signal and background samples and require a 5σ significance.

The discovery potential for this signal is shown in Fig. 6 for the largest and smallest energy loss by the R-hadron considered in our modelling of the R-hadron interaction with the detector. For both choices of this interaction, the discovery potential is smallest for high probabilities of producing the R_g^0, and it increases with the probability of producing an R-meson. This is because there can be significant missing transverse energy when a neutral R-hadron is produced together with a charged one. If the charged R-hadron is considered to be a jet with a non-isolated muon, this gives a jet and significant missing transverse energy. This also explains why the model of the interaction with less energy loss gives a lower signal: if the charged R-hadrons deposit less energy in the calorimeter, they are more likely to be considered as leptons and not included in the analysis, which reduces the signal.

Even using this model of low interaction with the detector, gluinos with masses up to $1.1\,\mathrm{TeV}$ can be discovered with $100\,\mathrm{fb}^{-1}$ integrated luminosity, and gluinos with masses up to $1.3\,\mathrm{TeV}$ can be observed with an integrated

Table 4. Allowed values for each of the cuts described in the text. In each case the variable is required to be larger than the value quoted

Variable						Allowed values					
$\not{E}_{\mathrm{T}}$	[GeV]	100	150	200	300	400	600	800	1000	1500	2000
$P_{\mathrm{T}_{j_1}}$	[GeV]	100	150	200	300	400	600	800	1000	1500	2000
$P_{\mathrm{T}_{j_2}}$	[GeV]	50	100	150	200	300	400	500	600	800	1000
$\sum P_{\mathrm{T}_j}$	[GeV]	100	200	300	400	500	600	800	1000	1500	2000
N_{jet}		2	3	4	5	6	7	8	9	10	11
S_{T}		0	0.1	0.2	0.3	0.4	0.5	0.6	0.7	0.8	0.9
$\Delta\phi_{j_1}$		0	0.3	0.6	0.9	1.2	1.5	1.8	2.1	2.4	2.7
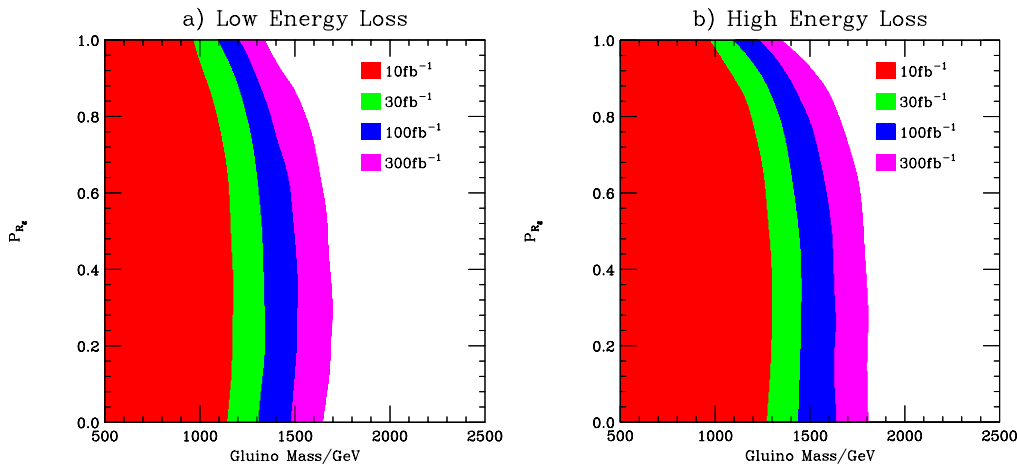
Fig. 6. Discovery reach for the missing transverse energy plus jets signal. Panel **a** shows the discovery potential using twice the interaction length and the triple-pomeron form of the cross section, which leads to the smallest energy loss by the R-hadron. Panel **b** shows the search reach using half the R-hadron interaction length and the cut-off form of the cross section, which leads to the largest energy loss by the R-hadron

luminosity of $300\,\mathrm{fb}^{-1}$[4]. The main difference between the searches for charged and neutral R-hadrons is that in the missing transverse energy search we will not be able to measure the gluino mass except through the total cross section. However, this might be possible for gluino masses of $\mathcal{O}(\mathrm{TeV})$, if we look for gluino–gluino bound states leading to a peak in the two-jet invariant mass spectrum [32].

4 Yukawa couplings from gaugino–Higgsino mixing

If split supersymmetry should be realized in nature, the observation of the gluino, charginos and neutralinos will only be the first task. Once these states are discovered, we will have to show that they constitute a weak-scale SUSY Lagrangean. At the LHC, the immediate challenge will be the determination of the quantum numbers of the new particles [33]. Even if we take for granted their fermionic nature, this does not establish them as SUSY partners: the set of color-octet, weak isosinglet, isotriplet, and a pair of isodoublet fermions (as present in the MSSM) makes up a minimal non-trivial extension of the standard model that is anomaly-free and consistent with gauge coupling unification. A quantitative hint for supersymmetry is given by the off-diagonal elements in the mass matrices. They determine the mixing of gauginos and higgsinos into charginos and neutralinos as mass eigenstates. This mixing is possible because supersymmetry transformations maintain standard model quantum numbers. These off-diagonal entries in the mass matrix also constitute the neutralino and chargino Yukawa couplings. In SpS, these off-diagonal entries follow, up to renormalization group effects, the predicted MSSM pattern.
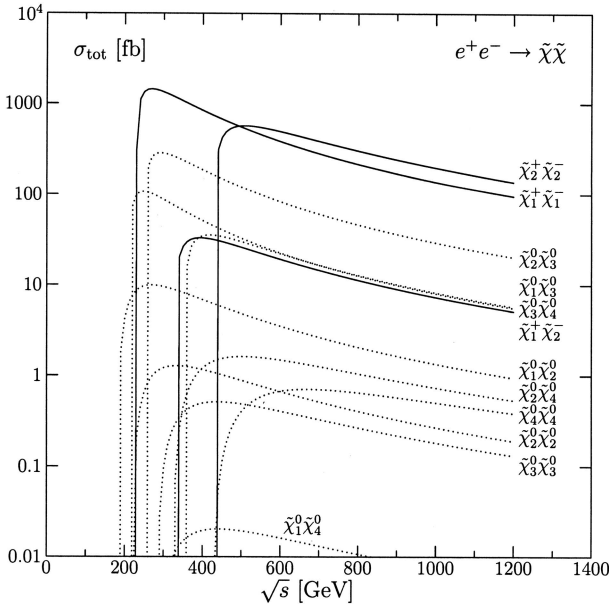
Without any mixing, the only production channels (in the absence of scalars) in $\bar{q}q$ or e^+e^- annihilation are $\tilde{\chi}_1^+\tilde{\chi}_1^-$,

$\tilde{\chi}_2^+\tilde{\chi}_2^-$, $\tilde{\chi}_1^\pm\tilde{\chi}_2^0$, $\tilde{\chi}_2^\pm\tilde{\chi}_{3,4}^0$, and $\tilde{\chi}_3^0\tilde{\chi}_4^0$. Moreover, all these produced particles would be stable. Any other production or decay channel requires either a finite coupling to s-channel gauge bosons through mixing or the presence of scalars. The observation of additional production channels and the measurement of decay branching ratios is therefore an indirect probe of the neutralino and chargino Yukawa couplings. The usual analysis of gauge couplings and the corresponding gaugino-sfermion-fermion couplings will fail in SpS scenarios, because the squarks are much heavier than the gauginos [34]. To measure the neutralino and chargino mixing matrices, a precise mass measurement is sufficient. Without gaugino–Higgsino mixing the mass matrices are determined by the MSSM parameters M_1, M_2 and μ. The gaugino–Higgsino mixing adds terms of the order of M_Z and introduces the additional parameter $\tan\beta$, leading to four MSSM parameters altogether. As shown before [35], these parameters can be extracted from the six neutralino and chargino masses by using a simple fit, properly including experimental errors [36].

Figure 7 displays the cross sections for chargino and neutralino pair production in e^+e^- collisions for the point of (2) as a function of the collider energy. With one exception, all channels have cross sections larger than 0.1 fb and the threshold value for $\tilde{\chi}_1^+\tilde{\chi}_1^-$ production is as large as 1 pb. A linear collider with moderate energy and high luminosity would be optimal to probe all these processes, and some kind of fit is the proper method to extract the weak-scale Lagrangean parameters. We emphasize that these cross sections [37] as well as the masses [16] are known to NLO. However, because we are mainly interested in the error on the extracted underlying parameters and less interested in their central values, we limit our fit to leading order observables.

Previous studies of the chargino and neutralino systems concentrated on the extraction of the mass parameters M_1, M_2, μ, while the off-diagonal elements were fixed or at least related to each other by the MSSM relations. In SpS, the four off-diagonal entries in the mass matrices are independent observables. As defined in (4) we parameterize the couplings $\tilde{g}_{u,d}^{(\prime)}$, introducing an additional factor $(1+$

---

[4] Recently, the interactions of the R-hadrons in the detector has been considered in more detail [31]. While the energy losses for the R-hadrons they find is generally within the broad range we consider they find a significant probablity of the conversion of mesonic into baryonic R-hadrons, which we have neglected and may reduce the discovery potential for charged R-hadrons.

Fig. 7. Cross sections for chargino and neutralino pair production in e^+e^- collisions [38], assuming the reference point in (2)

$\kappa_{u,d}^{(\prime)}$) with respect to the MSSM values [8]. While these κ parameters vanish to leading order in the complete weak-scale MSSM, the SpS renormalization flow between the matching scale $\widetilde{m}$ and the electroweak scale induces non-zero values of order $\kappa_i^{(\prime)} = -0.2 \ldots 0.2$. If we are able to detect deviations of this size at a collider, we can both establish the supersymmetric nature of the model and verify the matching condition to the MSSM at $\widetilde{m}$.

As mentioned above, the neutralino and chargino mixing matrices can be measured at a future linear collider, in continuum production as well as through a threshold scan [39]. The six masses alone are sufficient to determine all the usual MSSM parameters $M_1, M_2, \mu, \tan\beta$, plus one additional κ. Because the predicted values $\kappa_i^{(\prime)}$ are small, the correct treatment of the experimental accuracies is crucial. For our central parameter point of (2) we compute the masses and the cross sections shown in Fig. 7, with the exception of the $\tilde{\chi}_1^0 \tilde{\chi}_1^0$ channel. To all observables we assign an experimental error, which in our simplified treatment is a relative error of 0.5% on all linear-collider mass measurements [39], 5% on all LHC mass measurements [40], and the statistical uncertainty on the number of events at a linear collider corresponding to $100\,\mathrm{fb}^{-1}$ of data at a 1 TeV collider after all efficiencies[5]. The assumption that the LHC might be able to see all six gauginos and Higgsinos and measure all their masses is very optimistic, so we will only use it to derive the maximum sensitivity the LHC could achieve.

---

[5] Disentangling the various channels is a non-trivial task, but in the final fit it is always possible to replace the total cross sections by any other measurement. We leave this complication to a more detailed study of the experimental uncertainties [39] and the proper correlated fit including statistical, systematical and theoretical errors [41].

Moreover, the precision of the theoretical cross section prediction [17] and the precision of the measurement of cross sections and branching ratios at the LHC is likely to be insufficient to allow the extraction of small mixing parameters. Around the central parameter point we randomly generate 10000 sets of pseudo-measurements, using a Gaussian smearing. Out of each of these sets we extract the MSSM parameters. In principle, we could simply invert the relation between the masses and the Lagrangean parameters analytically. However, after smearing, this inversion will not have a unique and well-defined solution; therefore we use a fit to solve the overconstrained system. The distribution of the 10000 fitted values should return the right central value and the correctly propagated experimental error on the parameter determination. If necessary, we apply another maximum χ^2 cut on the 10000 fits, to get rid of secondary minima. The distributions of the measurements are not necessarily Gaussian, and there might be non-trivial correlations between different measurements. At the end, the crucial questions are the following.
(i) Is the error on the parameter measurements sufficient to claim agreement with the MSSM prediction?
(ii) Is the measurement good enough to probe the renormalization group effects of the heavy scalars in SpS?

As a first test of our approach we set all four non-MSSM contributions to zero ($\kappa_i^{(\prime)} = 0$) and add one of the four anomalous Yukawa couplings to the set of fitted parameters, keeping the other three fixed during the fit. In Fig. 8 we show the result for a combined fit of M_1, M_2, μ, κ_u and possibly $\tan\beta$. At a linear collider we can extract the mass parameters at the percentage level and the best measured anomalous coupling, κ_u, to typically 0.01. In Table 5 we see that the error on the determination of all four κ values at a linear collider is a few per cent. Generically, the error on $\kappa_d^{(\prime)}$ is larger than the error on $\kappa_u^{(\prime)}$, because $\kappa_d^{(\prime)}$ is accompanied by $\cos\beta$ while $\kappa_u^{(\prime)}$ enters with an additional factor $\sin\beta$. We checked that for large $\tan\beta$ values, e.g. $\tan\beta = 30$, only $\kappa_u^{(\prime)}$ can be extracted with a reasonable error. If we fix all but one κ to their zero MSSM prediction, the remaining off-diagonal entries in the mass matrices are determined by $\tan\beta$. While we might hope to extract $\tan\beta$ from the Higgs sector, we also test the prospects of determining it in our fit. In Table 5 we see that errors only slightly degrade when we include $\tan\beta$ in the set of parameters we fit to, and in Fig. 8 we see that the determination of $\tan\beta$ indeed works very well.

Since we are limiting the number of unknowns to four or five (depending on whether or not we fit $\tan\beta$), the six mass measurements should be sufficient to extract one anomalous Yukawa coupling parameter. Indeed, in Table 5 we see that the precision on the $\kappa_i^{(\prime)}$ suffers only slightly when we limit our set of measurements to the masses alone and assume $\tan\beta$ to be known. This is an effect of the overwhelming precision of the mass measurement through threshold scans, our assumed error of 0.5% is even conservative. Adding $\tan\beta$ to the fit shows, however, that with five parameters and six measurements our analyses are starting to lose sensitivity. When we try to extract the Lagrangean
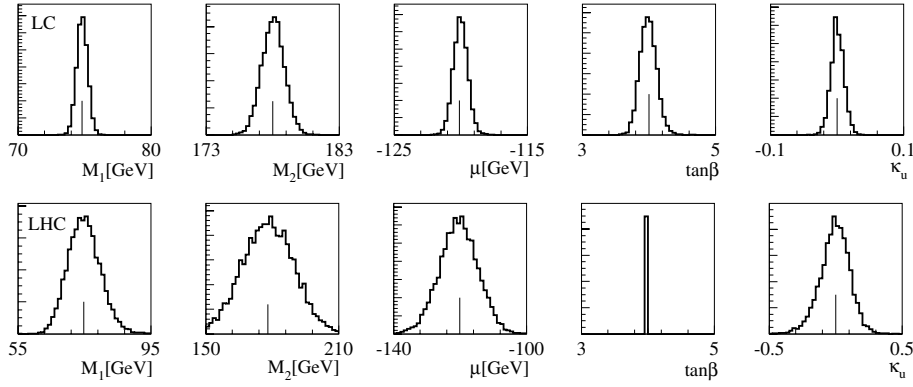
Fig. 8. Fit to 10000 sets of mass and cross section pseudo-measurements at a future linear collider (upper) and at the LHC (lower). The fitted parameters include only κ_u with a central value zero. At the LHC $\tan\beta = 4$ is fixed

Table 5. Error on the determination of κ_i from measured masses and possibly production cross sections. For the first five lines, all but one κ are fixed to zero; the fitted κ has the central value zero. In the last four lines, all four κ_i are fitted simultaneously. The very last line assumes the predicted central values of κ_i in our SpS parameter point. The error on the mass measurements is 0.5% for Tesla and 5% for the LHC. The sets of measurements marked by * include a maximum χ^2 cut to get rid of secondary minima

	Fit $\tan\beta$	m_i	σ_{ij}	$\Delta\kappa_u$	$\Delta\kappa_d$	$\Delta\kappa_u'$	$\Delta\kappa_d'$
Tesla		●	●	0.9×10^{-2}	3×10^{-2}	1.3×10^{-2}	4×10^{-2}
Tesla	●	●	●	1.2×10^{-2}	5×10^{-2}	2×10^{-2}	5×10^{-2}
Tesla		●		1.1×10^{-2}	5×10^{-2}	3×10^{-2}	8×10^{-2}
Tesla	●	●		1.2×10^{-2}	11×10^{-2}	4×10^{-2}	8×10^{-2}
LHC		●		2.2×10^{-1}	6×10^{-1}	2.7×10^{-1}	8×10^{-1}
Tesla		●	●	1.4×10^{-2}	5×10^{-2}	3×10^{-2}	10×10^{-2}
Tesla*	●	●	●	1.7×10^{-2}	9×10^{-2}	4×10^{-2}	13×10^{-2}
Tesla	fix $\tan\beta = 3$	●	●	1.6×10^{-2}	4×10^{-2}	4×10^{-2}	9×10^{-2}
Tesla*	$\kappa_i \neq 0$	●	●	1.4×10^{-2}	5×10^{-2}	4×10^{-2}	11×10^{-2}

parameters from a set of mass measurements at the LHC, the errors on the mass parameters M_1, M_2, μ inflate to the $10\% \dots 20\%$ level, as shown in Fig. 8. While we might still be able test if the $\kappa_u^{(\prime)}$ follow the weak-scale MSSM prediction, the experimental precision is clearly insufficient to test the SpS renormalization group effects. Moreover, it is not clear if all neutralino and chargino masses could be extracted at the LHC, because all current search strategies rely on squark and gluino cascade decays [40]. Last but not least, we do not know if we will be able to measure $\tan\beta$

in the Higgs sector, and including $\tan\beta$ in the LHC fit will make the extraction of $\kappa_u^{(\prime)}$ even less promising.

At the linear collider, adding the cross sections as independent measurements allows us to fit all four $\kappa_i^{(\prime)}$ simultaneously. This is the proper treatment, unless we would have reasons to believe that some of the $\kappa_i^{(\prime)}$ are predicted to be too small to be measured. This means that $\tan\beta$ is no longer an independent parameter: we can fix it in the fit, to reduce the number of unknown Lagrangean parameters. The error on the determination of all four $\kappa_i^{(\prime)}$ is shown in Fig. 9, including the error on M_2, to illustrate that adding
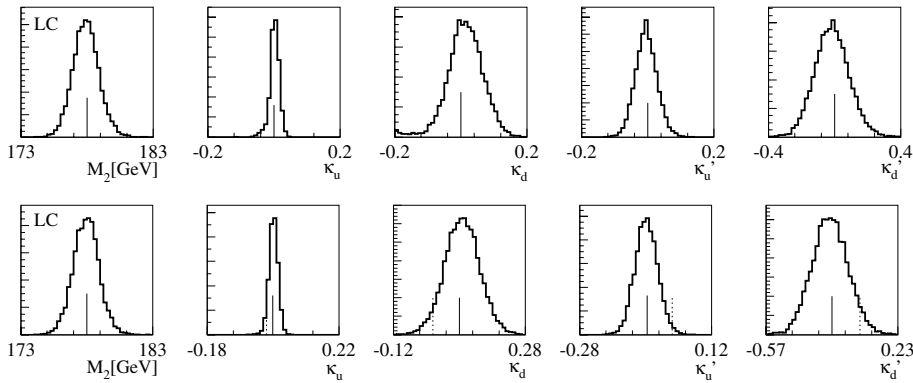
Fig. 9. Fit to 10000 sets of mass and cross section pseudo-measurements at a future linear collider. All four $\kappa_i^{(\prime)}$ are extracted simultaneously. The central values are set to zero as in the MSSM (upper) and to the example SpS values (lower). The MSSM zero prediction is indicated in the lower line of histograms

all four anomalous couplings to the fit has little impact on the measurement of the dominant Lagrangean mass parameters. In Table 5 the errors for the simultaneous κ measurements are compared with the single-κ fit. If we fix $\tan\beta$ to the correct value, the error bands increase by a factor of 2.5 at the maximum, when we move to a combined extraction of all $\kappa_i^{(\prime)}$. Adding $\tan\beta$ to the fit shows us to which degree we are already limited by the number of useful measurements: the quality of the measurements suffers considerably and we have to avoid secondary minima. However, as we already pointed out, $\tan\beta$ should be fixed if we limit ourselves to independent parameters. The question is: what happens if we fix it to a wrong value? From (4) we see that assigning a wrong value to $\tan\beta$ should just move the central values of the extracted $\kappa_i^{(\prime)}$, in our case away from zero. As an example, for an assumed value $\tan\beta$ the four anomalous coupling measurements are centred around $0.023, -0.23, 0.023, -0.23$ instead of zero, in the order of Table 5. Again in Table 5 we see that the effect on the errors is indeed negligible.

The last step left is from the case $\kappa_i^{(\prime)} = 0$ to the values predicted by SpS, (4). This is merely a cross-check, because the error in the extraction of the anomalous couplings should not significantly depend on their central values. Indeed, in Fig. 9 and in Table 5 we see that the central value has no visible effect on the errors, even though in our case it makes the fit more vulnerable to secondary minima. As usual, we get rid of the secondary minimum using a maximum-χ^2 value for the 10000 pseudo-measurements, reducing the number of entries in the histogram by 17%. These results for the linear collider indeed indicate that we could not only confirm that the Yukawa couplings and the neutralino and chargino mixing follow the predicted MSSM pattern; for the somewhat larger $\kappa_i^{\prime}$ values we can even distinguish the complete weak-scale MSSM from a SpS spectrum.

5 Direct measurement of Yukawa couplings

While the elements of the neutralino and chargino mixing matrices depend on the Yukawa couplings in a complicated way, the cross sections for chargino/neutralino pair production in association with a Higgs boson are directly proportional to these parameters. Therefore, the observation of $H\tilde{\chi}\tilde{\chi}$ final states [38, 42] could add to our knowledge of the Yukawa couplings that can be gained in chargino/neutralino pair production.

If decays of the kind $\chi_2^\pm \to \chi_1^\pm H$ or $\chi_j^0 \to \chi_i^0 H$ proceed with a significant rate, these branching fractions are determined by the Yukawa couplings in conjunction with the mixing effects and should be included in a global fit. Unfortunately, for low values of the mass parameters M_1, M_2, μ this is less likely to happen than in the MSSM, since the Higgs is considerably heavier, so that some channels are no longer kinematically accessible. In particular, for the reference point (2), no such decay is possible.

However, in this situation there is still associated production of charginos and neutralinos with a Higgs boson
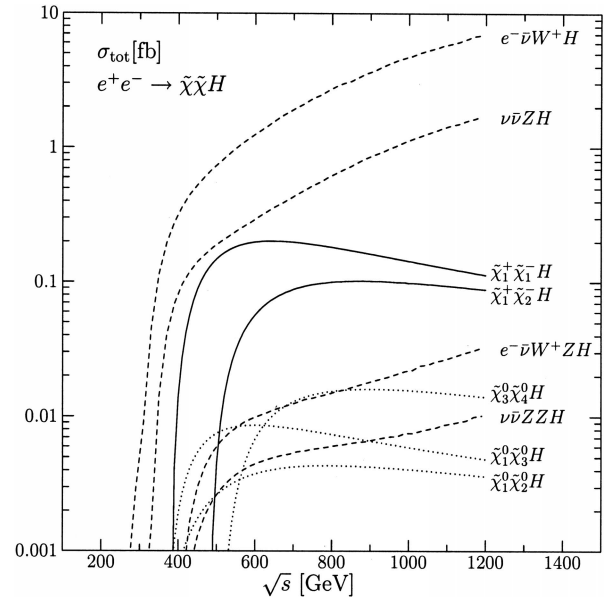
Fig. 10. Signal and background cross sections for associated production of neutralinos and charginos with a Higgs boson in e^+e^- collisions [38]

in the continuum, which can in principle be observed at a high-luminosity e^+e^- collider. Figure 10 displays the cross sections as a function of the collider energy. Like all s-channel processes, the curves peak immediately above the respective threshold energies. The dominant standard model background to these processes consists of Higgs production in association with Z and W bosons and a neutrino pair, also shown in Fig. 10. The neutrino pair can either originate from a Z boson or from the continuum (W-fusion processes), where in the latter case the total cross section increases with energy. Last but not least, we have to take into account processes with a forward-going electron in the final state, which may escape undetected.

Although the backgrounds are substantial, they do not affect all signals simultaneously, and they can be reduced significantly by kinematical cuts. Assuming thus that processes with Higgs-strahlung off a chargino or neutralino can be identified above the background, they will depend on the κ directly and through the neutralino and chargino masses. Apparently, the neutralino processes have a rate too small to help in disentangling the parameters. However, in contrast to chargino pair production, $\tilde{\chi}^+\tilde{\chi}^- H$ associated production depends on κ_u and is independent of $\kappa_u^{\prime}$, so its inclusion in a global fit reduces the correlation between these two parameters. Because the dependence of the cross sections on $\kappa_d^{\prime}$ is fairly weak, this parameter will pose a challenge for the direct extraction.

The precision that can be achieved from cross section measurements is given by the statistical error on the cross section. Assuming $1\,\mathrm{ab}^{-1}$ of integrated luminosity, we could collect a sample of at maximum 200 (100) signal events, which gives us an error of 7% (10%) on the cross section measurement and therefore an error of 3.5% (5%) on the measurement of the Yukawa coupling. This number could

be competitive with our estimates for the indirect measurement shown in Table 5. However, even if we can extract the masses involved using a threshold scan, the extraction of couplings from cross sections is always plagued by theoretical uncertainties due to higher orders and systematical experimental uncertainties. More detailed studies are required to obtain a final verdict on the errors [41].

6 Conclusions

Recently, models of split supersymmetry have been suggested. If we are willing to accept a high degree of fine-tuning for the separation between the weak scale and the Planck scale, decoupling of all sfermions can solve problems which usual supersymmetry has in the flavor sector, mediating proton decay or leading to large electric dipole moments. In particular, gauge coupling unification and the existence of a dark-matter candidate naturally survive the decoupling of the scalar partner states.

For collider experiments this means that only gauginos and Higgsinos are light enough to be produced, because their masses can be protected by a chiral symmetry. At the LHC we will observe a long-lived gluino. Over almost the entire parameter space, we will be able to see the resulting charged R-hadrons for gluino masses larger than 2 TeV and determine the gluino mass to better than 1%. In the region where the probability of producing a mesonic R-hadron is small, the reach can be enhanced by the classic jets plus missing-energy channel. In the case of neutral R-hadrons this leaves us with a reach of between 1.3 TeV and 1.8 TeV for the gluino mass, depending on the details of the R-hadron spectroscopy. Because we cover neutral as well as charged R-hadrons our result is independent of the mass hierarchy of the R-hadrons and the possible R-hadron decays into each other. We emphasize that the interaction of the gluino in the detector is currently being studied in more detail and we expect improved estimates for the discovery reach as well as for the mass measurement [31].

Because cascade decays of squarks and gluinos leading to subsequent neutralino and chargino signals will not be available for split-supersymmetry models, we give the direct production cross sections for all possible channels. It will be a challenge to extract these signals from the standard model backgrounds and separate them to gain access to some of the model parameters.

Obviously, a future high-luminosity linear collider will be perfectly suited for this kind of precision measurements. Integrating out the scalars at a high scale leads to renormalization group effects for the neutralino and chargino Yukawa couplings and their mixing matrices. At a linear collider we will be able to see all neutralinos and charginos and measure their masses and cross sections, provided the collider energy is sufficient. From these measurements we can extract the mixing matrix elements (with contributions from the anomalous Yukawa couplings) to better than 10% accuracy. The estimate of the experimental errors is based on a similar parameter point studied in [39]. For a final statement about the possible accuracy with which we can extract the anomalous Yukawa couplings one would have to

combine a detector simulation with the proper treatment of the theoretical errors, which is beyond the scope of this paper. Through the associated production of charginos with a Higgs boson we might also have direct access to these Yukawa couplings. If split-supersymmetry effects are large enough we will be able not only to confirm that neutralinos and charginos are indeed the partners of gauge bosons and Higgs bosons – we will also gain insight into the heavy decoupled spectrum.

References

1. ATLAS Collaboration, TDR, vol. 2, CERN-LHCC/99-015 (1999); CMS Collaboration, CERN-LHCC/94-38 (1994)
2. L. Alvarez-Gaumé, J. Polchinski, M.B. Wise, Nucl. Phys. B **221**, 495 (1983); L.E. Ibañez, Phys. Lett. B **118**, 73 (1982); J.R. Ellis, D.V. Nanopoulos, K. Tamvakis, Phys. Lett. B **121**, 123 (1983); K. Inoue, A. Kakuto, H. Komatsu, S. Takeshita, Prog. Theor. Phys. **68**, 927 (1982) [Erratum **70**, 330 (1983)]; A.H. Chamseddine, R. Arnowitt, P. Nath, Phys. Rev. Lett. **49**, 970 (1982)
3. M. Dine, W. Fischler, M. Srednicki, Nucl. Phys. B **189**, 575 (1981); S. Dimopoulos, S. Raby, Nucl. Phys. B **192**, 353 (1981); C.R. Nappi, B.A. Ovrut, Phys. Lett. B **113**, 175 (1982); L. Alvarez-Gaumé, M. Claudson, M.B. Wise, Nucl. Phys. B **207**, 96 (1982); M. Dine, A.E. Nelson, Phys. Rev. D **48**, 1277 (1993); M. Dine, A.E. Nelson, Y. Shirman, Phys. Rev. D **51**, 1362 (1995); M. Dine, A.E. Nelson, Y. Nir, Y. Shirman, Phys. Rev. D **53**, 2658 (1996)
4. For an overview, see e.g. M. Drees, S.P. Martin, hep-ph/9504324
5. G.R. Farrar, P. Fayet, Phys. Lett. B **76**, 575 (1978)
6. H. Baer, K.M. Cheung, J.F. Gunion, Phys. Rev. D **59**, 075002 (1999)
7. N. Arkani-Hamed, S. Dimopoulos, hep-th/0405159
8. G.F. Giudice, A. Romanino, hep-ph/0406088
9. S. Weinberg, Phys. Rev. Lett. **59**, 2607 (1987)
10. L. Susskind, hep-th/0405189
11. S. Dawson, H. Georgi, Phys. Rev. Lett. **43**, 821 (1979); M.B. Einhorn, D.R.T. Jones, Nucl. Phys. B **196**, 475 (1982)
12. A. Arvanitaki, C. Davis, P.W. Graham, J.G. Wacker, hep-ph/0406034
13. A. Pierce, hep-ph/0406144; J.R. Ellis, T. Falk, G. Ganis, K.A. Olive, M. Schmitt, Phys. Rev. D **58**, 095002 (1998); for a recent review, see e.g. G. Bertone, D. Hooper, J. Silk, hep-ph/0404175
14. P.M. Ferreira, I. Jack, D.R.T. Jones, Phys. Lett. B **387**, 80 (1996); http://www.liv.ac.uk/~dij/betas
15. For a recent review, see e.g. S. Heinemeyer, hep-ph/0407244; R. Mahbubani, hep-ph/0408096

16. T. Fritzsche, W. Hollik, Eur. Phys. J. C **24**, 619 (2002); W. Oller, H. Eberl, W. Majerotto, C. Weber, Eur. Phys. J. C **29**, 563 (2003)
17. W. Beenakker, R. Höpker, M. Spira, P.M. Zerwas, Nucl. Phys. B **492**, 51 (1997); W. Beenakker, M. Klasen, M. Krämer, T. Plehn, M. Spira, P.M. Zerwas, Phys. Rev. Lett. **83**, 3780 (1999); Prospino2.0, http://pheno.physics.wisc.edu/~plehn
18. M. Mühlleitner, A. Djouadi, Y. Mambrini, hep-ph/0311167
19. M.S. Chanowitz, S.R. Sharpe, Phys. Lett. B **126**, 225 (1983)
20. M. Foster, C. Michael [UKQCD Collaboration], Phys. Rev. D **59**, 094509 (1999)
21. For a review, see e.g. M. Neubert, Phys. Rept. **245**, 259 (1994); M. Neubert, hep-ph/0001334
22. F. Buccella, G.R. Farrar, A. Pugliese, Phys. Lett. B **153**, 311 (1985)
23. B.C. Allanach, C.M. Harris, M.A. Parker, P. Richardson, B.R. Webber, JHEP **0108**, 051 (2001)
24. I. Hinchliffe, F.E. Paige, Phys. Rev. D **60**, 095002 (1999);
25. G. Corcella et al., JHEP **0101**, 010 (2001); G. Corcella et al., hep-ph/0210213
26. B.R. Webber, Nucl. Phys. B **238**, 492 (1984)
27. G. Karl, J. Paton, Phys. Rev. D **60**, 034015 (1999)
28. E. Richter-Was, hep-ph/0207355
29. ATLAS Collaboration, TDR, vol. 1, CERN-LHCC/99-014
30. A.J. Barr, C.G. Lester, M.A. Parker, B.C. Allanach, P. Richardson, JHEP **0303**, 045 (2003)
31. A.C. Kraan, hep-ex/0404001
32. J.H. Kühn, S. Ono, Phys. Lett. B **142**, 436 (1984); T. Goldman, H. Haber, Physica D **15**, 181 (1985); E. Chikovani, V. Kartvelishvili, R. Shanidze, G. Shaw, Phys. Rev. D **53**, 6653 (1996)
33. A.J. Barr, hep-ph/0405052
34. H.C. Cheng, J.L. Feng, N. Polonsky, Phys. Rev. D **57**, 152 (1998)
35. J.L. Feng, M.E. Peskin, H. Murayama, X. Tata, Phys. Rev. D **52**, 1418 (1995); S.Y. Choi, A. Djouadi, M. Guchait, J. Kalinowski, H.S. Song, P.M. Zerwas, Eur. Phys. J. C **14**, 535 (2000); S.Y. Choi, J. Kalinowski, G. Moortgat-Pick, P.M. Zerwas, Eur. Phys. J. C **22**, 563 (2001) [Addendum C **23**, 769 (2002)]; S.H. Zhu, hep-ph/0407072
36. V.D. Barger, T. Han, T.J. Li, T. Plehn, Phys. Lett. B **475**, 342 (2000); V.D. Barger, T. Falk, T. Han, J. Jiang, T. Li, T. Plehn, Phys. Rev. D **64**, 056007 (2001)
37. W. Oller, H. Eberl, W. Majerotto, Phys. Lett. B **590**, 273 (2004); T. Fritzsche, W. Hollik, hep-ph/0407095
38. W. Kilian, LC-TOOL-2001-039; Proceedings ICHEP 2002, Amsterdam; M. Moretti, T. Ohl, J. Reuter, hep-ph/0102195; http://www-ttp.physik.uni-karlsruhe.de/whizard
39. J.A. Aguilar-Saavedra et al. [ECFA/DESY LC Physics Working Group Collaboration], hep-ph/0106315; B.C. Allanach, G.A. Blair, S. Kraml, H.U. Martyn, G. Polesello, W. Porod, P.M. Zerwas, hep-ph/0403133
40. H. Bachacou, I. Hinchliffe, F.E. Paige, Phys. Rev. D **62**, 015009 (2000); B.C. Allanach, C.G. Lester, M.A. Parker, B.R. Webber, JHEP **0009**, 004 (2000)
41. R. Lafaye, T. Plehn, D. Zerwas, hep-ph/0404282; http://sfitter.web.cern.ch; see also http://www-flc.desy.de/fittino
42. G. Ferrera, B. Mele, hep-ph/0407108